

Soft Matter

Accepted Manuscript



This is an *Accepted Manuscript*, which has been through the Royal Society of Chemistry peer review process and has been accepted for publication.

Accepted Manuscripts are published online shortly after acceptance, before technical editing, formatting and proof reading. Using this free service, authors can make their results available to the community, in citable form, before we publish the edited article. We will replace this *Accepted Manuscript* with the edited and formatted *Advance Article* as soon as it is available.

You can find more information about *Accepted Manuscripts* in the [Information for Authors](#).

Please note that technical editing may introduce minor changes to the text and/or graphics, which may alter content. The journal's standard [Terms & Conditions](#) and the [Ethical guidelines](#) still apply. In no event shall the Royal Society of Chemistry be held responsible for any errors or omissions in this *Accepted Manuscript* or any consequences arising from the use of any information it contains.



Cellular uptake and intracellular fate of protein releasing bacterial amyloids in mammalian cells

Joaquin Seras-Franzoso^{a,b,c,†,‡,*}, Alejandro Sánchez-Chardi^{d,‡}, Elena Garcia-Fruitós^{c,a,b,&}, Esther Vázquez^{a,b,c}, and Antonio Villaverde^{a,b,c}

Received 00th January 20xx,
Accepted 00th January 20xx

DOI: 10.1039/x0xx00000x

www.rsc.org/

Bacterial Inclusion Bodies (IBs) are amyloid protein deposits that functionally mimic secretory granules from the endocrine system. When formed by therapeutically relevant proteins, they complement missing intracellular activities in jeopardized cell cultures, offering an intriguing platform for protein drugs delivery in substitutive therapies. Despite the therapeutic potential of IBs, their capability to interact with eukaryotic cells, cross the cell membrane and release their functional building blocks into the cytosolic space remains essentially unexplored. We have systematically dissected the process by which bacterial amyloids interact with mammalian cells. An early and tight cell membrane anchorage of IBs is followed by cellular uptake of single or grouped IBs of variable sizes. Although an important fraction of the penetrating particles are led to lysosomal degradation, biologically significant amounts of protein are released into the cytosol. In addition, our data suggest the involvement of the bacteria cell folding modulator DnaK in the release of functional proteins from these amyloid reservoirs. The mechanisms supporting the internalization of disintegrable protein nanoparticles revealed here offer clues to implement novel approaches for protein drug delivery based on controlled protein packaging as bacterial IBs.

Introduction

Around the expectations deposited onto nano devices for solving diverse medical challenges, nanotechnologies have concentrated powerful multidisciplinary approaches. A representative example is the fast development of material sciences that has resulted in the wide spectrum of currently available micro- and nanomaterials as carriers for drugs or imaging agents.^{1,2} These materials include organic composites (polymers, liposomes, self-assembling peptides and proteins) and inorganic structures (silica and other glass particles and metal particles) in a wide range of shapes and presentations, including spheres, tubes, wires, shells, crystals, capsules, and quantum dots, among others.³⁻⁸ The high diversity of these

new vehicles offers a plethora of potential applications in nanomedicine, but their precise performance in biological interfaces, and the mechanisms of cell uptake and subsequent intracellular trafficking are still neglected issues that deserve deeper investigation.

Among broad potential biomaterials, bacterial Inclusion Bodies (IBs) are non-toxic, fully biocompatible functional amyloid sub-micron particles, ranging from about 50 nm to 1000 nm. They are naturally formed by recombinant protein that self-organize in producing bacterial cells through stereospecific cross-molecular interactions.^{9,10} Like secretory granules in the endocrine system,¹¹ IBs can release functional protein under appropriate conditions^{12,13}. In addition, these bacterial amyloids show a high versatility in terms of size, morphology, stiffness, zeta potential and density.^{14,15} Interestingly, these properties can be easily modulated by the proper choice of the genetic background of the producing strain.¹⁴ Remarkably, about 20 % of the protein content of IBs corresponds to proteinase K-resistant amyloid fibers, conferring the mechanical stability to the particles¹⁶ and enabling them to be used as topographies in cell culture and tissue engineering.¹⁷⁻¹⁹ The rest of the IB material is composed by quasi-soluble, releasable protein species that confer the biological activity.^{20,21} In this regard, IBs have been adapted as “all in one” nanopills,^{12,22} based on their natural cell penetrability and on the sustained release of IB protein to the cytosol and nucleus of the uptaking cells. Essentially, any therapeutic protein species can be produced in bacteria and packaged as functional IBs.²³ The potential applicability of IBs in biological

^a Institut de Biotecnologia i de Biomedicina, Universitat Autònoma de Barcelona, Bellaterra, 08193 Barcelona, Spain.

^b Departament de Genètica i de Microbiologia, Universitat Autònoma de Barcelona, Bellaterra, 08193 Barcelona, Spain.

^c CIBER de Bioingeniería, Biomateriales y Nanomedicina (CIBER-BBN), Bellaterra, 08193 Barcelona, Spain

^d Servei de Microscòpia, Universitat Autònoma de Barcelona, Bellaterra 08193 Barcelona, Spain

† Equally contributed

* Corresponding author

‡ Present address: Cibim-Nanomedicine, Hospital Vall d'Hebron, Passeig de la Vall d'Hebron, 119-129, 08035, Barcelona, Spain

[&] Present address: Department of Ruminant Production, Institut de Recerca i Tecnologia Agroalimentàries (IRTA), 08140 Caldes de Montbui, Spain.

Electronic Supplementary Information (ESI) available: [details of any supplementary information available should be included here]. See DOI: 10.1039/x0xx00000x

interfaces is, in addition, supported by the successful production of IBs in endotoxin-free bacterial strains.²⁴ However, the biomechanics supporting IB-cell interaction, cell membrane crossing and resulting activities had never been explored, a fact that narrows the further tuning of the material for particular biomedical applications including potential cell-targeting.

In the present study we have characterized at the ultrastructural level IBs and their interaction with mammalian cells upon cell exposure. These new insights in bacterial amyloid particles architecture, internalization and subsequent protein release to the cell compartments will contribute to the advance in the versatile use of this emerging protein delivery platform for therapeutic applications.

Experimental

Bacterial strains and plasmids

Escherichia coli JGT4 (*clpA::kan*, *Sm^R*)²⁵ bacterial strain, referred to as ClpA⁺, was transformed with the pTVP1GFP expression plasmid. This plasmid encodes the VP1GFP model protein formed by the foot-and-mouth disease virus capsid protein fused to the green fluorescence protein (GFP) (GenBank accession number KM242650). The construct enables the deposition of fluorescent IBs during protein overexpression processes particularly favored in protein quality control defective mutants such as ClpA⁺ strain.

E. coli MC4100 strain (*araD139 Δ[argF-lac]* U169 rpsL150 relA1 flbB5301 deoC1 ptsF25 rbsR) was used for the fabrication of VP1GFP IBs and the derived arginine, glycine and aspartic acid (RGD) tripeptide defective VP1GFP named VP1GFP(RGE).

IB production and purification

IB production was performed in shake flask by adjusting the optical density at 550 nm (OD₅₅₀) at 0.05 and incubating the culture at 37 °C and 250 rpm till reaching an OD₅₅₀ of 0.5. At this point protein expression was induced by the addition of isopropyl β-D-1-thiogalactopyranoside (IPTG) at 1 mM and further incubation of the bacterial cell culture was carried out for 3 h at 37 °C and 250 rpm. IBs were purified through a combination of mechanical and enzymatic procedures as previously described¹⁹.

IB size determination

IBs size distribution was obtained by measuring the diameter of protein particles from SEM micrographs using the free software Image J. We measured a total of 190 VP1GFP(RGE) IB particles produced in *E. coli* MC4100 strain, 209 VP1GFP IB particles also produced in MC4100, and 222 VP1GFP particles produced in *E. coli* JGT4 strain. SEM samples were prepared as detailed in the field emission scanning electron microscopy (FESEM) section.

Cell maintenance

HeLa cells (human cervical adenocarcinoma; ATCC CCL-2) were routinely cultured in MEM α 10 % (v/v) fetal bovine serum (FBS, Gibco, UK) and 2 mM L-glutamine (Gibco, UK) at 5 % CO₂ at 37 °C in a humidified incubator. Cos-1 cells (transformed African green monkey kidney fibroblasts; ECACC catalogue no. 88031701) were routinely cultured in DMEM 10 % FBS (v/v) and 2 mM L-glutamine at 10 % CO₂ at 37 °C in a humidified incubator. PC12 cells (rat adrenal pheochromocytoma; ECACC catalogue no. 88022401) were routinely cultured in DMEM 10 % FBS (v/v) and 2 mM L-glutamine at 10 % CO₂ at 37 °C in a humidified incubator. Culture flasks and plates were previously coated with poly-Lysine by the incubation in a 100 µg/mL solution for 5 min at RT and further washing in PBS. HepG2 cells (human hepatocellular liver carcinoma; ATCC HB-8065) were routinely cultured in MEM α 10 % FBS (v/v) and 2 mM L-glutamine at 5 % CO₂ at 37 °C in a humidified incubator. MDA-MB-231 cells (human breast carcinoma; ATCC HTB-26) were routinely cultured in DMEM:Ham's F12 (1:1 mixture) 5 % FBS (v/v) and 6 mM L-glutamine at 5 % CO₂ at 37 °C in a humidified incubator. GL261 cells (mouse glioma; National Cancer Institute at Frederick) were routinely cultured in RPMI 10 % FBS (v/v) and 4 mM L-glutamine at 5 % CO₂ at 37 °C in a humidified incubator.

Flow cytometry

Single timepoint internalization assay: 3 × 10⁴ HeLa cells, 6 × 10⁴ GL261 cells, 3 × 10⁴ Cos-1 cells, 5 × 10⁵ PC12 cells, 6 × 10⁴ HepG2 cells and 8 × 10⁴ MDA cells were seeded per well in 24 well plates. After 24 h of incubation under the appropriate conditions (see cell maintenance section) 10 µg of fluorescent IBs were added and cell cultures further incubated for 24 h. After IB incubation cells were washed once in DPBS and treated for 15 min in trypsin 1 mg/mL. This "harsh" trypsin digestion was performed in order to completely remove the extracellular protein and detect only the signal coming from the endocytosed particles.²⁶ Trypsin was neutralized by the addition of 2 volumes of complete medium and samples centrifuged 5 min at 1400 rpm. Cell pellets were resuspended in 0.3 mL DPBS and analyzed using FACSCalibur flow cytometer (BD Biosciences, USA), data was processed using the Flowing Software. All conditions were performed in duplicate.

IB internalization kinetics: 3 × 10⁴ HeLa cells were seeded in 24 well plates and incubated for 24 h at 37 °C and 5 % CO₂. Prior to the addition of IBs, chloroquine (CQ) at 10 ng/µL (final concentration) was added when necessary and incubated during 1 h at 37 °C and 5 % CO₂ in order to block endosomal maturation and the subsequent lysosomal digestion of the endocytosed protein particles.

IBs were incubated during 0 h, 0.2 h, 0.5 h, 1 h, 3 h, 5 h and 24 h. After incubation samples were trypsinized as mentioned in the previous section and analyzed in FACSCanto (BD Biosciences, USA) and processed using BD FACSDiva 4.0 software. All conditions were performed in duplicate.

Cell uptake inhibition assay: 6 × 10⁴ HeLa cells were seeded per well in 24 well plates. After 24 h of incubation under the appropriate conditions (see cell maintenance section)

endocytosis inhibitors were added at the following concentrations: Chlorpromazine 20 μM (Sigma-Aldrich, USA), Nystatin 50 μM (Sigma-Aldrich, USA), 5-(N-ethyl-N-isopropyl) amiloride (EIPA) 100 μM (Sigma-Aldrich, USA), Cytochalasin D 20 μM (Sigma-Aldrich, USA), using serum free media OptiPro (Gibco, UK) for 1 h. Then 10 μg of fluorescent IBs were added and cell cultures further incubated for 4 h. Samples were trypsinized as previously described and analyzed in FACSCanto (BD Biosciences, USA). All conditions were performed in triplicates.

Confocal Laser Scanning Microscopy (CLSM)

Cultures of 2.7×10^5 HeLa cells were seeded in MatTek cell culture dishes and incubated at 37 °C 5 % CO_2 in a humidified incubator for 24 h. 35 μg of IBs were then added per dish and incubated for 3 h. Cell membrane and nuclei were stained and stacks were obtained as described elsewhere.²⁷

Scanning Electron Microscopy (SEM)

For IBs ultrastructure, IBs were filtered in a Nucleopore 0.2 μm membrane (Whatman, UK) and fixed in 2.5 % (v/v) glutaraldehyde (EM grade, Merck, Germany) in 0.1 M phosphate buffer (PB, pH 7.4) for 2 h at 4 °C, dehydrated in an ascending ethanol series and dried with CO_2 by a critical point dryer CPD 030 (Bal-Tec, Liechtenstein). Samples were mounted on adhesive carbon films (Ted Pella, USA), coated with gold (20 nm) and observed with an S-570 scanning electron microscope (Hitachi Ltd., Japan) at an accelerating voltage of 15 kV.

For HeLa-IBs ultrastructure, samples were fixed following conventional electron microscopy methods^{28,29} and observed as previously described for IBs.

Field Emission Scanning Electron Microscopy (FESEM)

IBs ultrastructure, GFP immunolocalization in IB-HeLa samples and fluorescence detection in IB-HeLa samples were performed in a FESEM Zeiss Merlin (Germany) operating at 2 kV. Detailed procedures about sample preparation and image acquisition can be found in Supplementary Material.

Transmission Electron Microscopy (TEM)

IB negative staining, GFP immunolocalization in IBs, IB-HeLa ultrastructure, and immunolocalization of GFP and DnaK in IB-HeLa samples were assessed in a TEM Jeol JEM-1400 (Jeol Ltd., Japan) operating at 80 kV. Detailed procedures about sample preparation and image acquisition can be found in Supplementary Material.

Statistical analyses

Significant differences between internalization of RGD and RGE IBs in HeLa cells were determined with Mann-Whitney U -test using the Past3 software. Significant differences were assumed at $p \leq 0.05$.

Statistical analysis of cell uptake inhibition assay was also carried out through Mann-Whitney U -test using the Past3 software. Significant differences were assumed at $p \leq 0.05$.

Results

IB architectonic dissection

IBs formed by the model protein VP1GFP were successfully produced and purified as pseudo spherical particles with a diameter comprised between 100 and 600 nm, peaking in the range between 200 and 400 nm (Figure 1 a and b). Under transmission electron microscopy (TEM) and scanning electron microscopy (SEM) IBs showed a rough surface formed by numerous pits and grooves (Figure 1 c and d), compatible with the porous nature of the material.³⁰ In addition, IB's immunolabeling and further observation by TEM (Figure 1 e) revealed significant amounts of the recombinant protein. The presence of the forming protein VP1GFP was also evident in the inner structure of the particles as it is shown in Figure 1 f. Interestingly, both, IB surface and particle core exhibited a non-homogeneous distribution of gold nanoparticles, linked to the specific antibody against GFP (Figure 1 e and f), envisaging a differential distribution of the protein species throughout the IBs. Moreover, our model bacterial amyloid particles were fully fluorescent (Figure 1 g), indicating proper folding of the embedded protein. Noteworthy, also the fluorescence intensity was heterogeneously distributed along the IB sections.

IB-Cell membrane interface

Interaction between IBs and cultured HeLa cells was analyzed. IBs did not promote any evident sign of toxicity upon their addition to the culture media, based on the qualitative comparison of cell density between controls and IB treated cell cultures as well as nuclear morphology evaluation performed by bright field microscopy and TEM respectively (data not shown). Besides, their presence did not influence cell distribution and morphology as showed in Figure 2 a and b. In addition, IBs established intimate interactions with cell membrane, observed by SEM but also by confocal microscopy during live screening of the process (Figure 2 c). In this sense, green fluorescence linked to IBs was clearly detected inserted in cell membranes (Figure 2 c). GFP was also immunolocalized in bacterial amyloids in close contact with HeLa cells displayed by SEM (Figure 2 d).

A deeper analysis of the IB-cell interaction revealed an early contact, since 30 min upon IB addition, with the sensing machinery of the cells. Cell probing elements like filopodia were broadly observed (Figure 3 a) and IBs established discrete contact points with them. At these contact points the cell membrane-protein particle interface seemed partially unstructured (Figure 3 b and c). This phenomenon might act as an anchorage of the IBs to the cell prior to the engulfment of such structures. In addition, filopodia hooked the protein particles at their tips independently of IB's size (Figure 3 d, e and f) and surrounded single or grouped particles (Figure 3 g and h).

IB uptake and intracellular fate

Despite the high affinity of IBs for cell membranes, the first completely internalized particles were not observed by TEM till 3 h after their addition to cell cultures (Figure 4). At longer incubation times, a significant number of IBs could be detected completely inside the cells usually enveloped by cell membrane. At 8 h and 24 h post-exposure, more than one particle per cell was usually observed. Interestingly, at 24 h, some of the IBs lost the endocytic vesicle membrane (Figure 4).

Fluorescence screening along the time, performed by flow cytometry, permitted to quantify the cellular uptake of these functional amyloids. Note that prior to the flow cytometry analysis extracellular protein was completely removed by a "harsh" trypsin digestion. Cells exhibited a steady increase in fluorescence until 5 h upon IB addition. Interestingly, this tendency slowed down and eventually reached a plateau as it is shown in Figure 4 a, green line.

Moreover, in presence of the lysosomal maturation inhibitor chloroquine (CQ) markedly higher amounts of IBs inside the cells were observed compared to cell cultures in absence of CQ (Figure 4 a, red line). Observing the IB uptake profile for both conditions, the curves followed the same pattern till 1 h of particle incubation. After this point, a much steeper slope was detected for IBs plus CQ samples, indicating that even though the addition of CQ does not affect the initial stages of the uptake process, namely IB-cell membrane adhesion and particle wrapping, it is generating a clear difference at longer incubation times. This difference is explained by the accumulation of fluorescent protein inside the cells since CQ prevent protein degradation in the lysosomes. Thus, in regular conditions, cells degraded most of the internalized protein particles, although detectable amounts remained in an active form. In order to validate the assay, CQ toxicity in HeLa cells was evaluated. Despite the addition of CQ cell viability was not severely affected as appreciated in the MTT assay presented in Figure 4 b. Besides, testing IB uptake in presence of specific inhibitors of endocytic pathways (Figure 5) we only observed a significant decrease in particle uptake in the case of EIPA and an important decrease in presence of cytochalasin D, both inhibitors of macropinocytosis while no difference or even a slightly increase in IB internalization was observed when cells were treated with nystatin or chlorpromazine specifically inhibiting caveolae and clathrin mediated endocytosis respectively.

Even though most of IBs were leaded to lysosomal degradation, part of the particles remained in the cell and they could be released to the cell cytosol as depicted in Figure 5. After prolonged incubation times, endocytic membranes resulted disintegrated (Figure 6 a and b). Similarly to what is described in section *IB-Cell membrane interface* unstructured regions of the vesicle membrane were detected in punctual contacts between the protein particle and the vesicle (Figure 6 c and Figure 1 S1). This behavior suggested an active involvement of IBs in the disruption process. Interestingly SEM micrographs revealed these bacterial amyloids, once inside HeLa cells, exhibiting a loose structure but maintaining their forming protein fully fluorescent (Figure 6 d). These

observations, coupled with the immunolabelling of the IB forming protein, disclosed that the protein particles released their building blocks to the cell cytosol (Figure 6 e). Additionally, the presence in IBs of the bacterial chaperone DnaK, a protein constituent of IBs and involved in protein disaggregation among other functions, was also detected (Figure 6 f and g).

In order to evaluate if IB uptake was restricted to HeLa cells, we evaluated the ability of diverse cell lineages to incorporate IBs by flow cytometry. While uptake indeed occurred in different cell lineages (Figure 6 h), the magnitude of the internalization was dependent on the nature of the cell type tested. In this regard, PC12 neuron-like cells and GL261 cells were less prone to incorporate protein particles than others cell lines such as Cos-1, HepG2 or MDA-MB-231 with kidney, liver and breast origin respectively.

Influence of functional motifs on IB uptake

Finally, we studied the influence of the IB forming protein sequence in the ultimate performance of the amyloid particle. In this regard, particle internalization of two distinct versions of VP1GFP IBs was assayed. It is important to note that VP1 domain contains the integrin binding tripeptide Arginine – Glycine – Aspartic acid (RGD). This motif was replaced by the non-functional version Arginine – Glycine – Glutamic acid (RGE).³¹ IBs formed by VP1GFP and its derived VP1GFP (RGE) mutant showed little difference in size distribution (Figure 6 i). Nevertheless, particle uptake was significantly higher for those particles containing the RGD tripeptide in their sequence (Figure 6 j). These results suggested that the RGD remained at least partially functional and accessible in the protein particle playing an active role in the interaction with cells and their subsequent uptake.

Discussion

The architectural analyses performed in the present study have revealed a complex supramolecular organization of IBs. Different patterns in GFP labelling and fluorescence intensity suggest the co-existence inside the same protein particle of regions with distinct protein packaging grades and/or in different folding states. These irregular distributions are supported by previous data showing that IBs can contain variable amounts of the forming protein in its secondary structure depending on the production conditions.³² Therefore, the heterogeneous distribution of protein in their native-like conformation would be the result of the highly dynamic process of IB deposition. The enrichment of these protein particles in native-like conformation would increase the efficiency of the biological activity of the IBs, especially relevant when envisaged as protein drug delivery platforms. On the cell context, particle uptake by mammalian cells is one of the main barriers to overcome in order to generate reliable platforms for drug delivery. Numerous routes can be involved in this process, even for a defined particle type, being: phagocytosis, clathrin-mediated endocytosis, caveolae-

mediated endocytosis and macropinocytosis the most well-known.³³ Even though, these processes still remain in many aspects lightly understood. In this sense, clathrin mediated endocytosis which is associated with receptor mediated endocytosis is generally the main pathway for the uptake of small (<200 nm) particles and follow a fast kinetic entrance.³⁴ Although discrete IBs could follow this pathway, the uptake kinetics observed by flow cytometry reveals a slow entrance profile, typical from non-specific endocytosis rather than receptor mediated endocytosis. Moreover, although also some IBs vesicles showed the typical caveolae-mediated endocytosis structures (Figure 1 SI), small invaginations of the cell membrane of around 50 nm in diameter, is not likely for this route to be the main entry pathway for IBs.³⁵ IBs size and the low frequency of the IBs observed in contact with classical caveolae invaginations reinforce this statement. Besides, phagocytosis is quite specific of determined cell lineages such as macrophages, dendritic cells, monocytes or neutrophils and it shows a characteristic engulfment of large elements forming what is known as phagocytic cup.³⁶ These structures were not detected in our samples. Thus, macropinocytosis postulates as the responsible for the considerable entrance of IBs into HeLa cells. Macropinocytosis is strongly supported by the observation of big evaginations comprising several IBs at once as well as cell regions showing membrane ruffling and the generation of flat cytosolic extensions that surrounded the bacterial amyloid particles (for additional images illustrating IB endocytosis see Figure 1 SI). These evidences are in accordance with the typical vesicles described for macropinocytosis endocytic pathway, characterized by their broad diversity in size and shape.^{37,38} Moreover, the specific inhibition of macropinocytosis detected through the use of both chemical inhibitors EIPA and cytochalasin D, and the scarce effect of clathrin and caveolae mediated endocytosis inhibitors, chlorpromazine and nystatin, confirmed the conclusion derived from the ultrastructural assessment. All these evidences allow concluding that IBs cell entry is carried out through the macropinocytic pathway.

A deeper view at the IB-cell membrane contacts depicted punctual disintegration of the lipidic bilayer, in both, cell membrane and vesicle membrane. The partial insertion of IBs into lipid membranes would explain the high adhesive capacity of these particles onto cells, IBs remain fully attached to cell surface after extensive washing, and would provide a stable anchorage to facilitate the further particle wrapping and internalization. These observations coupled with the physicochemical features of IBs would be in agreement with the latest computational data in the field, reviewed by Ding, HM and co workers³⁹. In this complete and recent revision, the mechanics for nanoparticle internalization by both simple penetration and endocytosis have been extensively discussed. Focusing on endocytosis, particle wrapping, defined by the descriptors wrapping degree and wrapping time, would be crucial for nanoparticle internalization. In this sense, it has been shown that parameters such as particle size, membrane – particle adhesion and particle rigidity deeply influence the wrapping process. From our observations, IBs are able to insert

into the membranes but their size prevent their direct penetration since the required external force driving particle translocation would be too high. Nevertheless, the partial insertion would provide adhesive capacity and enough time to facilitate wrapping. In addition, this mechanistic process is in agreement with the slow uptake profile detected for these amyloid particles. The capacity to get inserted into the cell membrane would be probably due to the IB particle complexity, containing hydrophobic and hydrophilic regions. Previous studies proved the amphiphilic nature of IBs, being able to adhere onto both hydrophilic and hydrophobic gold functionalized surfaces.¹⁴ On the other hand, particle rigidity also influences the final uptake. In this regard, it has been shown that very soft particles such vesicles, with high bending grades, are difficult to wrap. These particles would deform while being surrounded by the cell membrane making harder to completely wrap them.⁴⁰ In this sense, IBs possess relatively high young modulus values ranging from 5 to 10 MPa¹⁴ making them suitable to be completely wrapped.

Once inside the cells and despite part of the internalized particles are led to degradation, some IBs can escape from the endosomal vesicles. Probably, the previous avidity observed by IB to lipid membranes and the inherent leaky nature of macropinocytic vesicles⁴¹ would facilitate the crossing of the protein particles to the cell cytosol where the forming protein can be released to carry out their function as previously described.^{12,22,42}

The mechanism by which protein is disaggregated from the particle surface is still unclear although the physiology of IB formation offers certain hints in respect of the release process. In this regard, protein particle deposition results from a highly controlled and dynamic process in which numerous chaperones and proteases take part.^{43,44} Among the most important chaperones regulating the aggregation/disaggregation process it is found the Hsp70 family member DnaK. This chaperone has multiple functions in the protein quality network in *E. coli*, being especially interesting its function as a refolding modulator of aggregated protein.^{45,46} Moreover, it has been reported that this chaperone, when co-expressed as a folding enhancer in eukaryotic recombinant protein production systems, is able to increase the amount of soluble protein reducing the presence of protein insoluble deposits.⁴⁷ Noteworthy, DnaK has also been previously reported as a typical IBs contaminant.⁴⁸ Since DnaK has been previously shown able to carry out its chaperone activity in eukaryotic systems and being part of IB composition it is reasonable to speculate with a possible disaggregating/refolding action of the remaining DnaK in the IBs internalized by HeLa cells.

IBs have proved able to be uptaken by distinct cell lineages. Despite the efficiency of the process seem to depend on the nature of the cell type, the general trend is that these particles can be uptaken in biologically relevant amounts by most of the cell lines tested. This characteristic opens the possibility of using this protein delivery platform for therapies requiring the targeting of different cell types. As expected, cells growing in floating clusters such as PC12 presented lower particle uptake

than adherent well spread cells such as HeLa or Cos-1. This result is in accordance with previous studies performed with polystyrene microspheres in which cells in suspension revealed lower uptake capacity compared to adherent cells.⁴⁹ Nevertheless, other parameters such as receptor density on the cell membrane⁵⁰, the metabolic state⁴⁹, or cell cycle phase⁵¹ that differs from one cell line to another can play important roles in particle internalization. Thus, although the general trend is that IBs are able to be uptaken by most cell lines a case per case study should be performed in order to optimize the particle features for the maximum internalization yield.

Finally we have also shown that this uptake process can be modulated by the forming protein engineering in a bottom-up manner. The protein nature of the IBs allows engineering the forming protein, adding or removing new functionalities to the peptide backbone and increasing therefore the plasticity of the resulting particles. In this regard, differences due to a punctual mutation destroying the cell-binding RGD motif resulted in a difference in the final particle performance. RGD motif has been extensively related to integrins as a specific ligand with high relevance in cell adhesion but also as a selective ligand for the functionalization of drug delivery systems towards tumor cells.^{52,53} In absence of this tripeptide, IBs' interaction with HeLa integrins would be hindered, decreasing the adhesion of VP1GFP(RGE) IBs to the cell membrane and reducing the cellular uptake. The influence of RGD in IB- cell binding is reinforced by the previous observation of strong cell adhesion onto IBs functionalized surfaces generated by the same model protein.^{17,19} It has been shown that cells growing on IB patterned surfaces can form mature focal adhesions suggesting that such surfaces facilitate integrin clustering and the subsequent focal adhesion formation.¹⁸ This IB unique versatility is advantageous respect to other inorganic micro/nano-materials and opens intriguing possibilities regarding the use of IBs as platforms for the delivery of therapeutic proteins such as the possibility to incorporate other peptide ligands for specific targeting or increase the efficiency of the endosomal escape by the incorporation of endosomal escape motifs. The last mentioned functionality would turn out crucial to avoid the marked lysosomal degradation and therefore would allow reaching higher protein concentrations in the targeted subcellular compartment.

Conclusions

IBs are complex sub-micron protein particles that intimately attach to mammalian cell membranes, being able to partially insert into the bilipid layer. This anchorage provides stability for the further wrapping of the particle and uptake, following the macropinocytic pathway. Once inside the cells IBs can disrupt the endosomal vesicles releasing their forming protein to the cell cytosol.

Besides, the protein nature of IBs can be exploited to tune the particle performance by engineering the polypeptide sequence at the genetic level. In our case disruption of RGD motifs in IBs

decreased particle internalization. This high plasticity would allow designing accurate strategies for specific applications in the biomedical field.

Acknowledgements

The authors acknowledge the financial support granted to E.G.F from INIA, MINECO, Spain (RTA2012-00028-C02-02), to A.V from Agència de Gestió d'Ajuts Universitaris i de Recerca (2014SGR-132) and from the Centro de Investigación Biomédica en Red (CIBER) de Bioingeniería, Biomateriales y Nanomedicina financed by the Instituto de Salud Carlos III with assistance from the European Regional Development Fund. A.V. has been distinguished with an ICREA ACADEMIA Award and JSF is recipient of a post-doctoral fellowship from Asociación Española Contra el Cáncer (AECC) and EGF received a post-doctoral fellowship from INIA (DOC-INIA, INIA, MINECO).. We are also indebted to "Servei de Microscopia" and "Servei de Cultius Celulars Anticossos i Citometria" (SCAC) from Universitat Autònoma de Barcelona (UAB) and to the Protein Production Platform (CIBER-BBN) for helpful technical assistance (<http://www.bbn.ciber-bbn.es/programas/plataformas/equipamiento>). We also thank to University of Turku for the free providing of Flowing Software and Dr. Nerea Roher for assistance in the inhibition of endocytic pathways assay.

Notes and references

- Bogart, L. K., Pourroy, G., Murphy, C. J., Puentes, V., Pellegrino, T., Rosenblum, D., Peer, D., and Levy, R., *ACS Nano.*, 2014, **8**, 3107-3122
- Duncan, R. and Richardson, S. C., *Mol.Pharm.*, 2012, **9**, 2380-2402
- Kastl, L., Sasse, D., Wulf, V., Hartmann, R., Mircheski, J., Ranke, C., Carregal-Romero, S., Martinez-Lopez, J. A., Fernandez-Chacon, R., Parak, W. J., Elsasser, H. P., and Rivera, Gil P., *ACS Nano.*, 2013, **7**, 6605-6618
- Nativo, P., Prior, I. A., and Brust, M., *ACS Nano.*, 2008, **2**, 1639-1644
- Giudice, J., Jares-Erijman, E. A., and Leskow, F. C., *Bioconjug.Chem.*, 2013, **24**, 431-442
- Plummer, E. M. and Manchester, M., *Mol.Pharm.*, 2013, **10**, 26-32
- Wang, T. and Jiang, X., *ACS Appl.Mater.Interfaces.*, 2013, **5**, 1190-1196
- Gratton, S. E., Ropp, P. A., Pohlhaus, P. D., Luft, J. C., Madden, V. J., Napier, M. E., and DeSimone, J. M., *Proc.Natl.Acad.Sci.U.S.A*, 2008, **105**, 11613-11618

- 9 Marston, F. A., *Biochem.J.*, 1986, **240**, 1-12
- 10 King, J., Haase-Pettingell, C., Robinson, A. S., Speed, M., and Mitraki, A., *FASEB J.*, 1996, **10**, 57-66
- 11 Maji, S. K., Perrin, M. H., Sawaya, M. R., Jessberger, S., Vadodaria, K., Rissman, R. A., Singru, P. S., Nilsson, K. P., Simon, R., Schubert, D., Eisenberg, D., Rivier, J., Sawchenko, P., Vale, W., and Riek, R., *Science*, 2009, **325**, 328-332
- 12 Vazquez, E., Corchero, J. L., Burgueno, J. F., Seras-Franzoso, J., Kosoy, A., Bosser, R., Mendoza, R., Martinez-Lainez, J. M., Rinas, U., Fernandez, E., Ruiz-Avila, L., Garcia-Fruitos, E., and Villaverde, A., *Adv.Mater.*, 2012, **24**, 1742-1747
- 13 Seras-Franzoso, J., Peebo, K., Luis, Corchero J., Tsimbouri, P. M., Unzueta, U., Rinas, U., Dalby, M. J., Vazquez, E., Garcia-Fruitos, E., and Villaverde, A., *Nanomedicine.(Lond)*, 2013, **8**, 1587-1599
- 14 Diez-Gil, C., Krabbenborg, S., Garcia-Fruitos, E., Vazquez, E., Rodriguez-Carmona, E., Ratera, I., Ventosa, N., Seras-Franzoso, J., Cano-Garrido, O., Ferrer-Miralles, N., Villaverde, A., and Veciana, J., *Biomaterials*, 2010, **31**, 5805-5812
- 15 Peternel, S., Jevsevar, S., Bele, M., Gaberc-Porekar, V., and Menart, V., *Biotechnol.Appl.Biochem.*, 2008, **49**, 239-246
- 16 Morell, M., Bravo, R., Espargaro, A., Sisquella, X., Aviles, F. X., Fernandez-Busquets, X., and Ventura, S., *Biochim.Biophys.Acta*, 2008, **1783**, 1815-1825
- 17 Seras-Franzoso, J., Diez-Gil, C., Vazquez, E., Garcia-Fruitos, E., Cubarsi, R., Ratera, I., Veciana, J., and Villaverde, A., *Nanomedicine.(Lond)*, 2012, **7**, 79-93
- 18 Seras-Franzoso, J., Tsimbouri, P. M., Burgess, K. V., Unzueta, U., Garcia-Fruitos, E., Vazquez, E., Villaverde, A., and Dalby, M. J., *Nanomedicine.(Lond)*, 2014, **9**, 207-220
- 19 Seras-Franzoso, J., Steurer, C., Roldan, M., Vendrell, M., Vidaurre-Agut, C., Tarruella, A., Saldana, L., Vilaboa, N., Parera, M., Elizondo, E., Ratera, I., Ventosa, N., Veciana, J., Campillo-Fernandez, A. J., Garcia-Fruitos, E., Vazquez, E., and Villaverde, A., *J.Control Release*, 2013, **171**, 63-72
- 20 Cano-Garrido, O., Rodriguez-Carmona, E., Diez-Gil, C., Vazquez, E., Elizondo, E., Cubarsi, R., Seras-Franzoso, J., Corchero, J. L., Rinas, U., Ratera, I., Ventosa, N., Veciana, J., Villaverde, A., and Garcia-Fruitos, E., *Acta Biomater.*, 2013, **9**, 6134-6142
- 21 Wang, L., Maji, S. K., Sawaya, M. R., Eisenberg, D., and Riek, R., *PLoS.Biol.*, 2008, **6**, e195
- 22 Liovic, M., Ozir, M., Bedina, Zavec A., Peternel, S., Komel, R., and Zupancic, T., *Microb.Cell Fact.*, 2012, **11**, 67
- 23 Villaverde, A., Garcia-Fruitos, E., Rinas, U., Seras-Franzoso, J., Kosoy, A., Corchero, J. L., and Vazquez, E., *Microb.Cell Fact.*, 2012, **11**, 76
- 24 Rueda, F., Cano-Garrido, O., Mamat, U., Wilke, K., Seras-Franzoso, J., Garcia-Fruitos, E., and Villaverde, A., *Appl.Microbiol.Biotechnol.*, 2014,
- 25 Thomas, J. G. and Baneyx, F., *J Bacteriol*, 1998, **180**, 5165-5172
- 26 Richard, J. P., Melikov, K., Vives, E., Ramos, C., Verbeure, B., Gait, M. J., Chernomordik, L. V., and Lebleu, B., *J.Biol.Chem.*, 2003, **278**, 585-590
- 27 Pesarrodonna, M., Ferrer-Miralles, N., Unzueta, U., Gener, P., Tatkiewicz, W., Abasolo, I., Ratera, I., Veciana, J., Schwartz S Jr, Villaverde, A., and Vazquez, E., *Int.J.Pharm.*, 2014, **473**, 286-295
- 28 Julian, E., Roldan, M., Sanchez-Chardi, A., Astola, O., Agusti, G., and Luquin, M., *J.Bacteriol.*, 2010, **192**, 1751-1760
- 29 Sanchez-Chardi, A., Olivares, F., Byrd, T. F., Julian, E., Brambilla, C., and Luquin, M., *J.Clin.Microbiol.*, 2011, **49**, 2293-2295
- 30 Taylor, G., Hoare, M., Gray, D. R., and Marston, F. A. O., *Bio-Technology*, 1986, **4**, 553-557
- 31 Suehiro, K., Smith, J. W., and Plow, E. F., *J.Biol.Chem.*, 1996, **271**, 10365-10371
- 32 Doglia, S. M., Ami, D., Natalello, A., Gatti-Lafranconi, P., and Lotti, M., *Biotechnol.J.*, 2008, **3**, 193-201
- 33 Medina-Kauwe, L. K., Xie, J., and Hamm-Alvarez, S., *Gene Ther.*, 2005, **12**, 1734-1751
- 34 Rejman, J., Oberle, V., Zuhorn, I. S., and Hoekstra, D., *Biochem.J.*, 2004, **377**, 159-169
- 35 Parton, R. G. and Simons, K., *Nat.Rev.Mol.Cell Biol.*, 2007, **8**, 185-194
- 36 Strijbis, K., Tafesse, F. G., Fairn, G. D., Witte, M. D., Dougan, S. K., Watson, N., Spooner, E., Esteban, A., Vyas, V. K., Fink, G. R., Grinstein, S., and Ploegh, H. L., *PLoS.Pathog.*, 2013, **9**, e1003446
- 37 Swanson, J. A. and Watts, C., *Trends Cell Biol.*, 1995, **5**, 424-428
- 38 Amyere, M., Mettlen, M., Van Der Smissen, P., Platek, A., Payrastra, B., Veithen, A., and Courtoy, P. J., *Int.J.Med.Microbiol.*, 2002, **291**, 487-494
- 39 Ding, H. M. and Ma, Y. Q., *Small*, 2015, **11**, 1055-1071

ARTICLE

Journal Name

- 40 Yi, X., Shi, X., and Gao, H., *Phys.Rev.Lett.*, 2011, **107**, 098101
- 41 Wadia, J. S., Stan, R. V., and Dowdy, S. F., *Nat.Med.*, 2004, **10**, 310-315
- 42 Seras-Franzoso, J., Peebo, K., Garcia-Fruitos, E., Vazquez, E., Rinas, U., and Villaverde, A., *Acta Biomater.*, 2014, **10**, 1354-1359
- 43 Martinez-Alonso, M., Vera, A., and Villaverde, A., *FEMS Microbiol.Lett.*, 2007, **273**, 187-195
- 44 Carrio, M. M. and Villaverde, A., *J Biotechnol*, 2002, **96**, 3-12
- 45 Rinas, U., Hoffmann, F., Betiku, E., Estape, D., and Marten, S., *J.Biotechnol.*, 2007, **127**, 244-257
- 46 Schlieker, C., Tews, I., Bukau, B., and Mogk, A., *FEBS Lett.*, 2004, **578**, 351-356
- 47 Martinez-Alonso, M., Toledo-Rubio, V., Noad, R., Unzueta, U., Ferrer-Miralles, N., Roy, P., and Villaverde, A., *Appl.Environ.Microbiol.*, 2009, **75**, 7850-7854
- 48 Carrio, M. M. and Villaverde, A., *J.Bacteriol.*, 2005, **187**, 3599-3601
- 49 Zauner, W., Farrow, N. A., and Haines, A. M., *J.Control Release*, 2001, **71**, 39-51
- 50 Wang, S. and Dormidontova, E. E., *Phys.Rev.Lett.*, 2012, **109**, 238102
- 51 Kim, J. A., Aberg, C., Salvati, A., and Dawson, K. A., *Nat.Nanotechnol.*, 2012, **7**, 62-68
- 52 Barczyk, M., Carracedo, S., and Gullberg, D., *Cell Tissue Res.*, 2010, **339**, 269-280
- 53 Dunehoo, A. L., Anderson, M., Majumdar, S., Kobayashi, N., Berkland, C., and Siahaan, T. J., *J.Pharm.Sci.*, 2006, **95**, 1856-1872

Figure Legends

Figure 1. Inclusion Body architecture. a) Size distribution of VP1GFP IBs produced in the ClpA⁻ *E. coli* strain. b) Overview of IBs population by SEM. c) and d) IB detail displayed by TEM and SEM respectively. e) GFP immunolabelling on whole particles displayed by TEM. f) GFP labelling on lowicryl section observed by TEM. g) SEM fluorescence micrograph of IB in lowicryl sections. Scale bar on panel b) corresponds to 2 μm while scale bars on the panels below size 200 nm.

Figure 2. Inclusion Bodies in the cell context. a) SEM micrographs showing HeLa cells in absence (IB -) and in presence (IB +) of IBs in the cell culture media. b) Magnifications showing HeLa cell surface without and with IBs respectively. c) GFP detection showing 3D reconstruction by CLSM of HeLa cells with IBs and the cross section of HeLa cell culture supplemented with IBs. d) GFP labelling detected by SEM. White arrows indicate gold nanoparticles. Scale bars in panel a) size 20 μm , while measure 2 μm in their magnifications, panel b). Scale bar in confocal cross section, panel c), represents 10 μm and 1 μm in SEM immune detection panels, panel d).

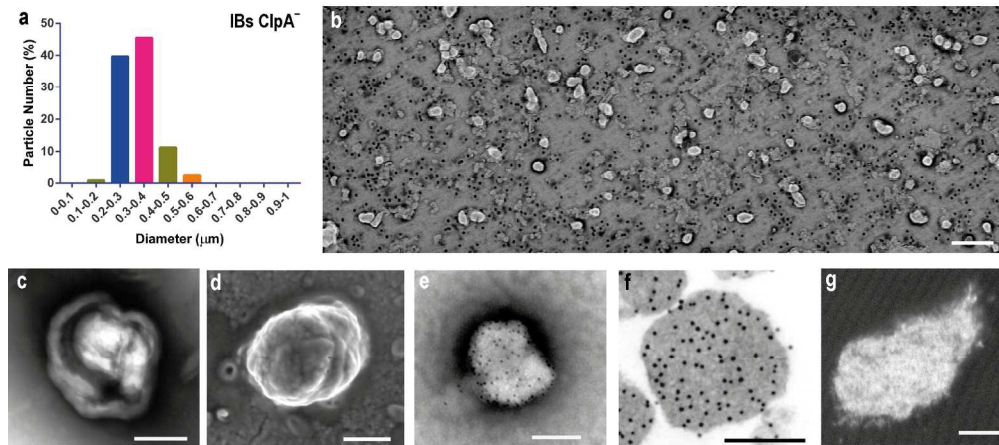
Figure 3. Insights of Inclusion Body – cell interface. a) SEM micrograph showing IB and cell filopodia interaction. b) and c) TEM image at high magnification showing disruption of cell membrane for IB anchorage. d – f) SEM and TEM images showing in detail the contact between IB and cell filopodia g) SEM micrograph showing macropinocytosis of IB groups in HeLa. h) GFP-labeling showing IB protein in HeLa macropinocytic cavities comprising several particles. Scale bars represent 2 μm in panels a) and g), 1 μm in panel h), and 200 nm in the rest.

Figure 4. Inclusion Bodies uptake kinetics. TEM micrographs illustrating the IB endocytic pathway in HeLa cells at 0.5, 1, 3, 8 and 24 h, after the addition of the protein particles. TEM magnifications and TEM GFP immunolabeled samples are displayed in the panels below. Scale bars size 1 μm in all the panels while represents 200 nm in magnifications. a) Uptake kinetics of IBs in HeLa cells. Mean fluorescence intensity (MFI) was measured by flow cytometry. Green line shows uptake kinetics for VP1GFP IBs while red line represents VP1GFP IBs uptake in presence of the lysosomal maturation inhibitor chloroquine (CQ). Inset shows IB uptake process at shorter incubation times. b) Cell viability assay of HeLa cells cultured in medium supplemented with VP1GFP IBs and VP1GFP IBs plus CQ.

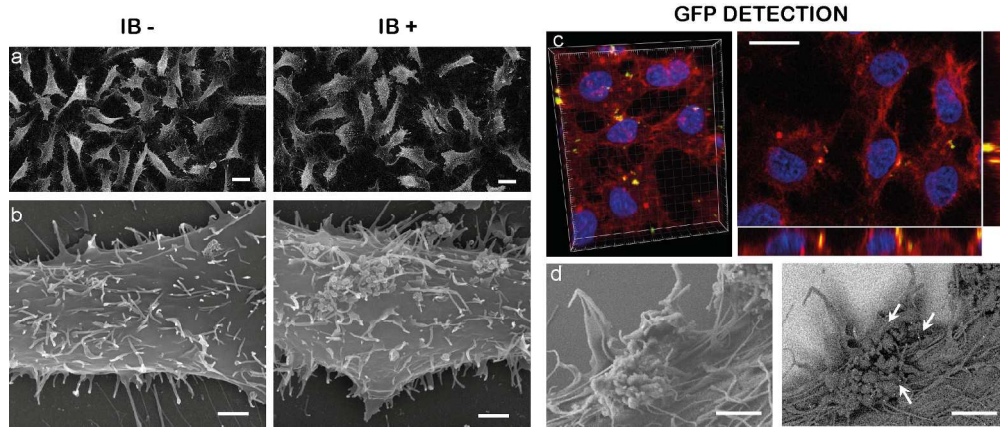
Figure 5. Chemical inhibition of endocytic pathways. Relative fluorescent cells after the treatment with chemical inhibitors of endocytic pathways: EIPA, Cytochalasin D, Nystatin and Chlorpromazine. * indicates $p \leq 0.05$.

Figure 6. Inclusion Body intracellular fate. a) TEM micrograph showing a general view of endocytosed IBs. b) TEM micrograph of GFP labelling in HeLa cells uptaking IBs. IB forming protein can be observed in the IBs inside macropinosomes c) TEM detail displaying endocytosed IBs being released to the cell cytoplasm. d) SEM fluorescence image illustrating the IB forming protein integrated in the cell cytoplasm maintaining their biological activity. e) TEM micrograph of GFP labelling in HeLa cells displaying endocytosed IBs releasing their forming protein to the cell cytoplasm. f) and g) TEM double labelling images (GFP and DnaK) showing the presence of both functional proteins in IBs after protein particle uptake. Black arrows mark 10 nm gold nanoparticles corresponding to GFP labelling while red arrows indicate 20 nm nanoparticles corresponding to DnaK labelling.

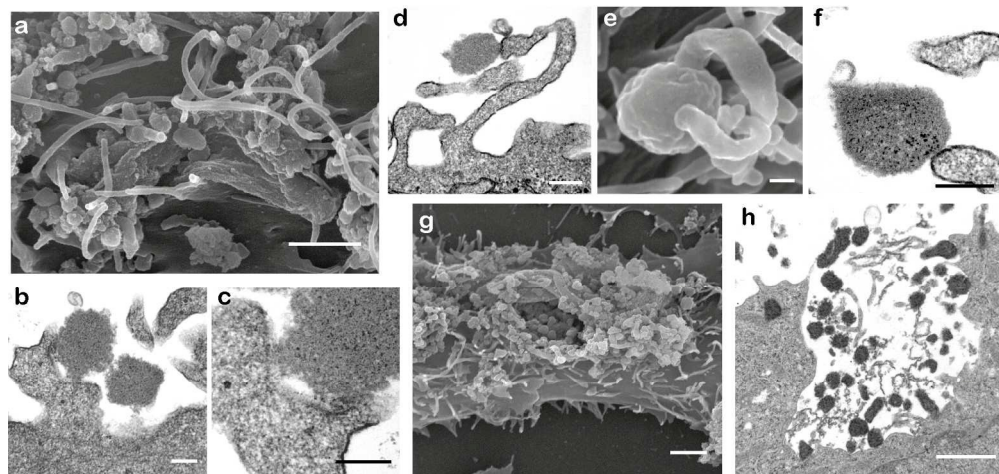
Scale bar size 1 μm in panel a), 500 nm in panel d), 200 nm in panels b), c), e) and g) and 100 nm in panel f). h) IB uptake efficiency tested by flow cytometry in several cell lines i) Size distribution of VP1GFP and VP1GFP(RGE) IBs produced in the MC4100 *E. coli* strain indicated as RGD and RGE respectively. j) Uptake of VP1GFP and VP1GFP(RGE) IBs by HeLa cells. * indicates $p \leq 0,001$.



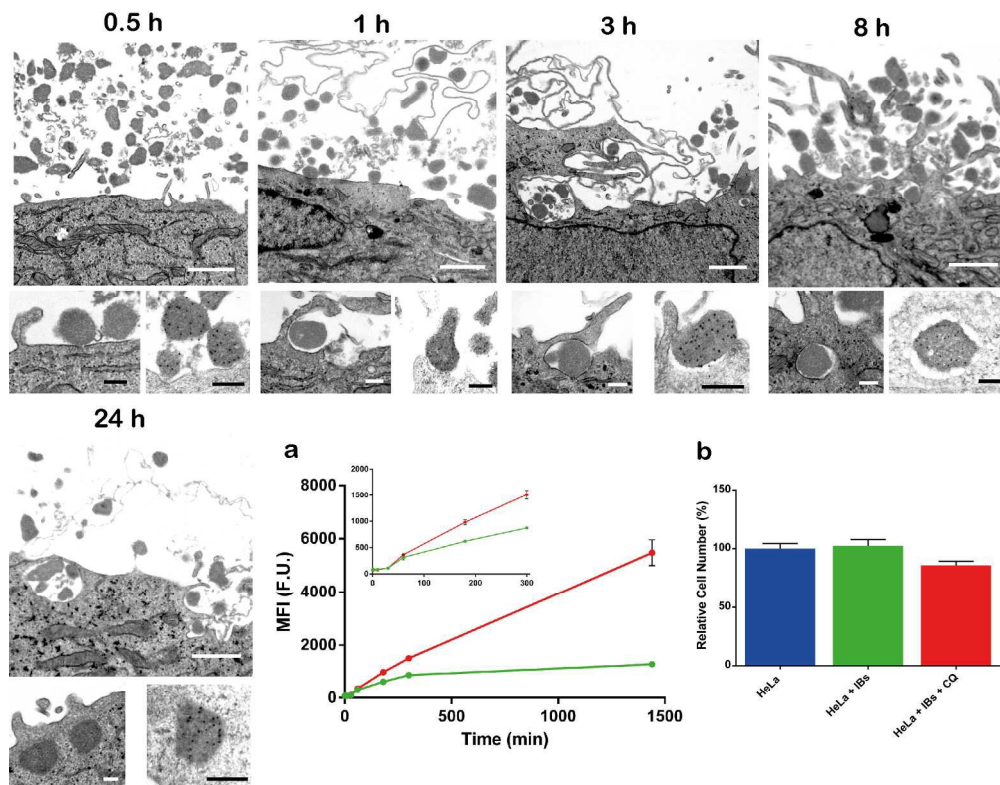
186x84mm (300 x 300 DPI)



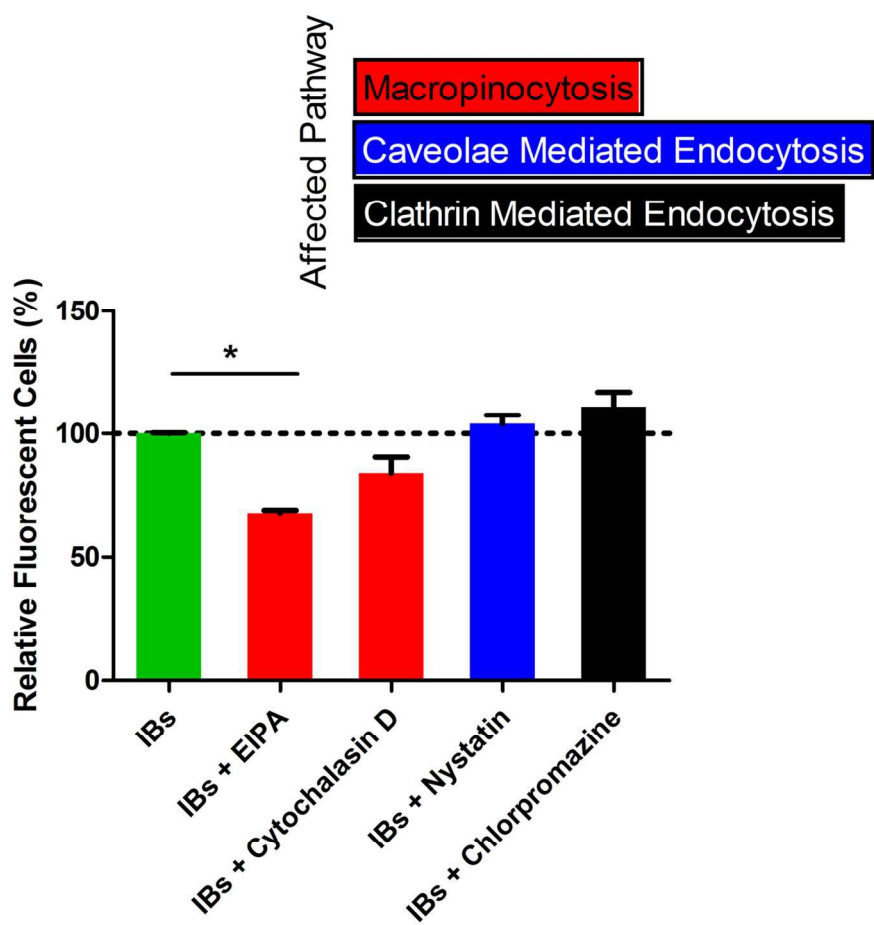
199x84mm (300 x 300 DPI)



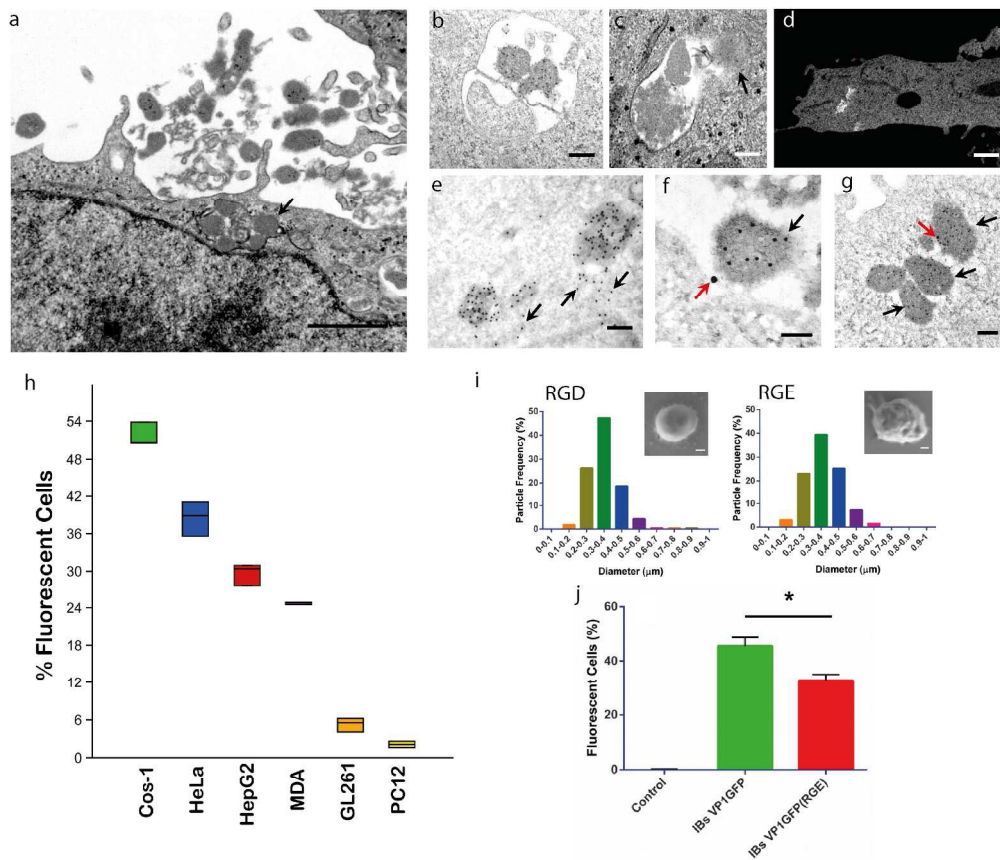
202x95mm (300 x 300 DPI)



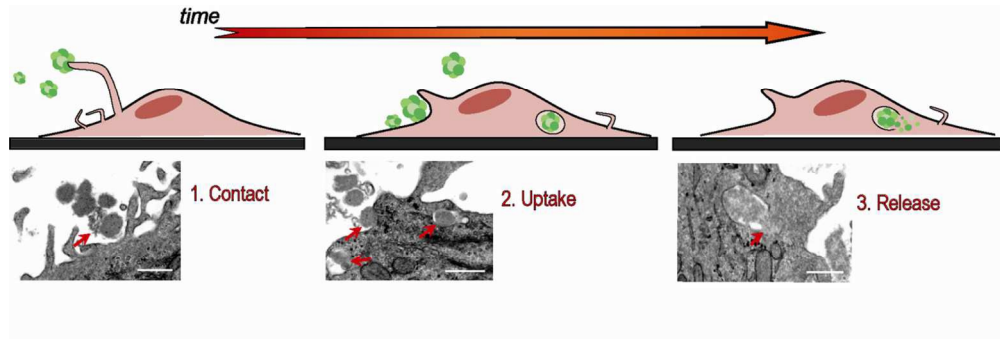
193x152mm (300 x 300 DPI)



131x125mm (300 x 300 DPI)



190x164mm (300 x 300 DPI)



112x37mm (300 x 300 DPI)